Combinatorial Investigations of Interfacial Failure*

ALFRED J. CROSBY†, ALAMGIR KARIM, ERIC J. AMIS

Polymers Division, National Institute of Standards and Technology, Gaithersburg, Maryland 20899

Received 25 October 2002; revised 13 January 2003; accepted 16 January 2003

ABSTRACT: Conventional measurements of interfacial strength focus on a single variable, whereas many variables couple nontrivially and simultaneously to define this property. We present a combinatorial methodology that allows the effects of multivariable environments on interfacial strength to be investigated in a high-throughput, parallel, and quantitative manner. This technique is largely based on the theory of Johnson, Kendall, and Roberts that quantifies adhesion through the contact and separation of a spherical lens and flat substrate. For our experiments, we fabricated a combinatorial library consisting of a two-dimensional array of spherical caps and a complementary substrate. The array of spherical caps was brought into contact and subsequently separated from the substrate, whereas the relative displacement and contact area of the individual lenses were recorded. With gradient library-fabrication methods, two adhesion-controlling parameters can be continuously varied along the orthogonal axes of the array. In this manner, each lens quantifies the interfacial strength at a unique point in parameter space. We demonstrate this multilens contact-adhesion test by measuring the effect of temperature and coating thickness on the self-adhesion of polystyrene thin films. © 2003 Wiley Periodicals, Inc. J Polym Sci Part B: Polym Phys 41: 883–891, 2003

Keywords: adhesion; thin films; fracture; polystyrene

INTRODUCTION

Combinatorial methodologies provide the user with a set of tools to evaluate a large parameter space optimally in a short period of time. Over the last decade, these powerful methods of experimental design have accelerated the development and optimization of new drugs in the pharmaceutical industry, and recently the "combi" way of thinking has begun in the field of materials science.[1,2] Early efforts in materials science largely focused on applying combinatorial methodologies to aid in the development of new materials; however, combinatorial methodologies have an equal or greater potential to play a significant role in the characterization and measurement of material properties.[3,4] Polymer adhesion is an important area of materials science that could be impacted by combinatorial methodologies. Polymer adhesion governs the performance of critical components in numerous industries including electronic packaging, automotive, biomedical, aerospace, and (of course) office supplies. Although polymer adhesion is controlled effectively in many situations, our understanding of the fundamental mechanisms of adhesion is elementary. Conventional experiments have focused on a single variable's effect on adhesion, whereas many variables such as surface energy, molecular weight, temperature, and contact geometry couple nontrivi-

*Certain equipment and instruments or materials are identified in this article to adequately specify the experimental details. Such identification does not imply recommendation by National Institute of Standards and Technology

†*Present address:* University of Massachusetts, Dept. of Polymer Science and Engineering, Conte Research Center, 120 Governors Drive, Amherst, MA 01003

Correspondence to: A. J. Crosby (E-mail: crosby@mail.pse.umass.edu)

Journal of Polymer Science: Part B: Polymer Physics, Vol. 41, 883–891 (2003)

ally and simultaneously to determine the overall polymer adhesion. We have developed a combinatorial methodology that allows the effects of multivariable environments on polymer adhesion to be investigated in a high-throughput, parallel, and quantitative manner. This new technique allows an upward of 1600 unique combinations of variables to be investigated in our configuration within the same time required for a single conventional adhesion experiment. This increase in throughput not only allows quantitative measurements of adhesion on an efficient timescale, but it also allows new areas of parameter space to be explored. These benefits will ultimately advance our fundamental ability to build predictive models of interface formation and failure. We present this combinatorial adhesion methodology and demonstrate quantitative high-throughput measures of the self-adhesion of polystyrene (PS) and the adhesive strength of polystyrene/poly(dimethylsiloxane) (PDMS) interfaces. Future research areas that can be investigated with this new experimental technique also are highlighted.

EXPERIMENTAL

Of the numerous techniques that exist for characterizing polymer adhesion, we have chosen to develop a combinatorial method on the basis of the theory of Johnson, Kendall, and Roberts (JKR).[5] This theory describes the quantification of the adhesion energy between two surfaces through the monitoring of the contact area ($A = \pi a^2$) during the contact and separation of a spherical cap with a flat substrate. The original form of the JKR equation is[5]

$$a^3 = \frac{9R}{16E}\left[P + 3\pi\mathcal{G}R + \sqrt{6\mathcal{G}RP + (3\pi\mathcal{G}R)^2}\right] \quad (1)$$

where R is the radius of curvature of the spherical cap, E is the elastic modulus of the contacting system, P is the applied force, and $\mathcal{G}$ is the work of adhesion. This equation can be rearranged to have the form of a fracture mechanics equation[6,7]

$$\mathcal{G} = \frac{3(P' - P)^2}{32\pi E a^3} \quad (2)$$

where the work of adhesion, $\mathcal{G}$, is equivalent to the energy-release rate for a propagating crack at the interface of the contacting system. For eq 2, $P' = 4Ea^3/[3R(1 - \nu^2)]$, the Hertzian contact force for a sphere contacted a plane with ν as Poisson's ratio.

Classically, the JKR technique/theory has been used to quantify the surface energy of soft, elastic solids, but in recent years, it has been extended to characterize the adhesive behavior of a wide spectrum of polymer interfaces including glassy polymers, elastomers, pressure-sensitive adhesives, and biological materials.[7–11] Additionally, the results of this technique correlate with other industrially recognized methods such as the peel test and the probe-tack method.[12,13] This demonstrated versatility provides the motivation for developing a combinatorial adhesion test on the basis of the JKR method.

Our combinatorial JKR test consists of an array of spherical caps (microlenses) that is brought into contact with a flat (complementary) substrate. Accordingly, this approach is referred to as a multilens contact adhesion test (MCAT). The contact area of each microlens with the complementary substrate is monitored with an optical microscope as a function of relative displacement during a controlled contact and separation process. Because the measurement of the force at each microlens contact point is difficult, we used a modified version of JKR theory to quantify the adhesion energy from the applied displacement and resulting contact radius[7]

$$\mathcal{G} = \frac{2E(\delta' - \delta)^2}{3\pi a} \quad (3)$$

where δ is the applied relative displacement, and $\delta' = a^2/R$, the Hertzian displacement for a contacting sphere and flat plane. Equations 1–3 are only applicable for geometrically unconfined systems. As the contact radius becomes comparable or greater than other length scales associated with the deforming body, correction factors must be applied to extend the applicability of the JKR theory.[7]

For a conventional MCAT experiment, we prepared our materials library such that two adhesion-controlling parameters vary along orthogonal axes and the experiment combinatorially maps the dependence of adhesion on these two parameters in a single test. This approach is demonstrated by testing the self-adhesion of PS and the adhesion of PS/PDMS interfaces as a function of temperature (T) and film thickness (h).

LIBRARY FABRICATION

To fabricate the PDMS microlens arrays used in this research, we used a replication molding technique similar to the methods applied for making PDMS stamps for soft-lithography processing.[14,15] In our process, we begin with a fused-silica microlens array that serves as a master. The fused-silica microlens array used in this work was purchased from MEMSOptical, Inc., but several manufacturers and processes exist for fabricating microlens arrays.[16–20] The specific pattern geometry or size scale of the microlens array used in this work is not necessary or specific for this combinatorial adhesion test. From the master microlens array, a PDMS negative mold was cast with Dow Corning's Sylgard 184 mixed in a 10:1 mass ratio of base-to-curing agent and cured at room temperature for 48 h. This PDMS negative was subsequently coated with a layer of approximately 10 nm of evaporated carbon. The carbon layer acts as a barrier layer for casting a PDMS-positive microlens array. From this PDMS microlens array, an epoxy negative mold is cast to expedite repeated fabrication of PDMS-positive microlens arrays. The PDMS microlens arrays are swollen in heptane for 12 h to remove uncrosslinked PDMS and subsequently air-dried for 30 h and under vacuum for 2.5 h at 60 °C.

For these tests, we fabricated a PDMS microlens array with each microlens having a diameter of 250 ± 1 μm, a radius of curvature of 366 ± 1 μm, and an edge spacing between microlenses of 10 ± 0.1 μm. With these dimensions, the microlens library contains approximately 1600 microlenses in a square centimeter area. These dimensions are not critical to the use of our method; however, they enable high-throughput imaging under an optical microscope and an easily accessible magnitude of applied force range for contact and separation.

To compare the adhesive strength of PS/PS and PS/PDMS interfaces, we created a combinatorial library consisting of a PDMS microlens array partially coated with a thin film of PS and a PS-coated Si wafer as the complementary substrate. Both uniform and gradient thickness PS coatings were cast from toluene solutions with a flow-coating technique whose details have been published.[3] The molecular mass of the PS used to coat both the Si wafer and the microlens array was 114,200 g/mol.[21] To coat the microlens arrays with PS, a PS solution was flow-coated onto a glass slide. This coated glass slide was slowly submerged into a bath of deionized water to allow the PS coating to be peeled off the glass slide and float at the air/water interface. This floating PS coating was subsequently picked up onto the microlens array. All PS coatings were air-dried for 24 h and annealed at 90 °C for at least 2 h on the microlens array. Specifically, the PDMS microlens array had a single-strip region coated with a 216 ± 10 nm thick PS film (Fig. 1). This library design exhibits two distinct interface regions upon contact—PS/PS interfaces within the PS-coated microlens region and PS/PDMS interfaces on either side of the strip region. Accordingly, our combinatorial adhesion test is designed to compare simultaneously the different levels of adhesion for these two polymer interfaces.

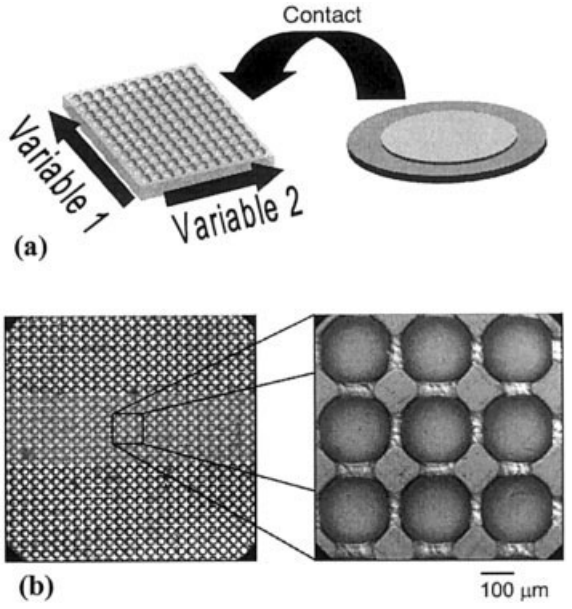

Figure 1. (a) Combinatorial library including microlens array and complementary substrate. (b) Optical microscope images of the top surface of a PDMS microlens array. Artificial shading in left image indicates region coated with PS film. Magnified image on right illustrates the conformal coating of floated PS coating stretched over individual PDMS microlenses.

The strip-coated PDMS microlens library was brought into contact with the PS-coated substrate at the controlled rate of 1 μm/s with an actuator-driven device. The adhesion test apparatus consists of a vertically positioned actuator fixed to an automated X-Y translation stage mounted on an optical microscope (Nikon Optiphot). We used National Instrument's Labview software to control the motion of the actuator, to record the displacement readings of the actuator's linear encoder,

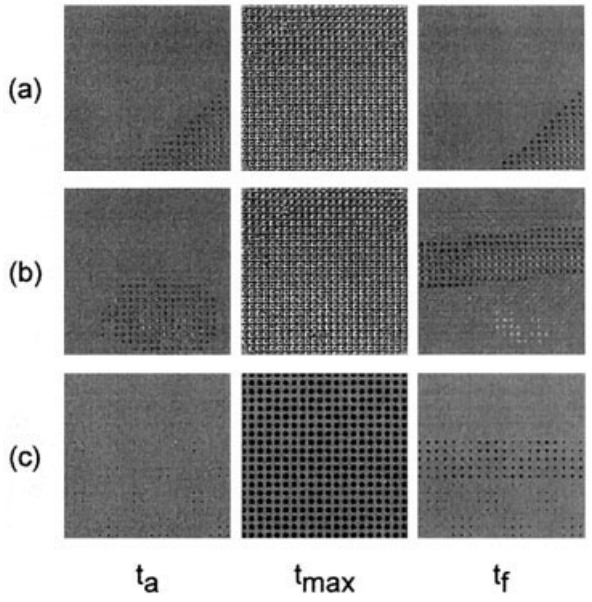

Figure 2. Images showing the contact areas of contacting microlenses within an array at different times during a test: t_a takes place during initial contact (approach), t_{max} is at maximum compression, and t_f is near final retraction of the microlens array. (a) PDMS microlens array coated with thin PS on the center rows contacting a PS-coated Si wafer at 25 °C, (b) same sample tested at 100 °C, and (c) image sequence produced by simple simulation on the basis of classical JKR theory for a planar array of soft spheres contacting a flat, rigid plane. Center rows of array are defined with higher interfacial adhesion ($\mathcal{G}$) values.

and to collect the images of contact areas between the microlens array and the coated Si substrate. Upon reaching a relative displacement where the microlenses were contacting the PS-coated Si wafer, the direction of motion was reversed at 1 μm/s until the library components resumed their initial separated state.

RESULTS

This test was conducted at two temperatures—25 and 100 °C. At 25 °C the contact areas, as monitored by optical microscopy, did not indicate any differences between the adhesion of the PS/PS and PS/PDMS interfaces [Fig. 2(a)]. However, at 100 °C the PS/PS interfaces remained in contact for an extended period of time during separation relative to the two surrounding PS/PDMS regions. This difference in contact history is evident by comparing the image sequences in Figure 2(a,b). At time t_a, the image portrays the microlenses coming into contact. At time t_{max}, the image exhibits the microlenses at the maximum point in compression. At time t_f, the image shows the contacting microlenses shortly before final detachment. In Figure 2(a), the microlens array is brought into contact at 25 °C. At this temperature, the order of contact upon approach is nearly identical to the order of contact upon retraction. This indifference in contact history for any region of the microlens array suggests that within the optical resolution of our test, no discernible difference in the adhesion of PS/PS and PS/PDMS interfaces at 25 °C is measured. The sensitivity of the adhesion measurement is dictated by the optical resolution of our image-capture device, the resolution of our linear actuators, the precision of our linear encoders, and the elastic properties of the contacting system. For these initial measurements, the instrument was not optimized for near-thermodynamic adhesion strengths. Now, a new instrument is being fabricated with this sensitivity and will be discussed in a future publication.

At 100 °C [Fig. 2(b)] the region of microlenses at initial contact (t_a) is clearly different from the last region of contact (t_f). The last region of contact is mainly confined to the region of the array where the PS/PS interfaces are located. This hysteresis in contact history is due to an increase in adhesion energy that is caused by an apparent increase in molecular diffusion and entanglement across the mobile PS/PS interface. As a consequence of this increased adhesion at 100 °C at the PS/PS interface, the PS coating on the PDMS microlenses fractured around the perimeter of the contact areas, and welded regions of PS from the coating on the microlens array were observed on the PS-coated Si wafer upon full retraction of the microlens array (Fig. 3). Because the PS/PS interface welding did not occur at 25 °C, a critical temperature must exist between 25 and 100 °C for developing the threshold PS/PS molecular adhesion during the specified contact time.

To explore this critical welding temperature, we used a high-throughput methodology in which a sample similar to the one described above was brought into contact with a PS-coated Si wafer on a temperature gradient stage[4] with 100 °C $< T <$ 80 °C. In this experiment, we observed that for a 216-nm-thick coating of PS on PDMS the transition to PS/PS welding occurs at approximately 89 $\pm$ 0.9 °C (Fig. 4). This temperature of 89 °C is below the glass-transition temperature (T_g) for

bulk PS where a significant increase in molecular diffusion may have been expected, thus suggesting that film thickness may play a role in the welding temperature. We repeated this test with the only modification being the thickness of the PS coating on the PDMS microlens array. For a coating thickness of 30 nm, the welding transition temperature is 75 °C, thus confirming a thickness dependence for this coating-failure mode.

To further explore this phenomenon, we created a library where the thickness (h) of the PS coating on the PDMS array varied along the film-length direction, and a temperature gradient (T) on the PS-coated wafer was applied in the orthogonal direction. As Figure 5 illustrates, the combinatorial adhesion test maps the trend of the critical welding temperature of PS self-adhesion as a function of film thickness for nearly 800 (h, T) combinations.

ANALYSIS AND DISCUSSION

Qualitatively, the continuous imaging of the contact areas provides a quick and simple assessment of the relative adhesion values across the surface of a combinatorial library. The areas where the microlenses remain in contact the longest are adhesively stronger relative to the areas

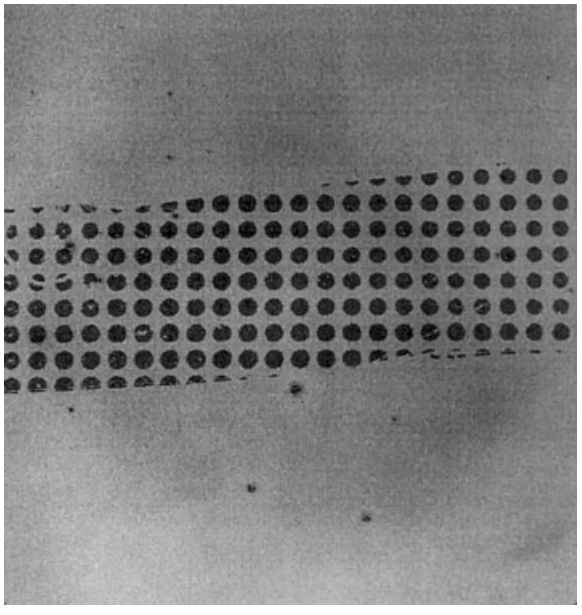

Figure 3. PS weld spots deposited on the PS-coated Si wafer after final detachment of a partially PS-coated microlens array at 100 °C.

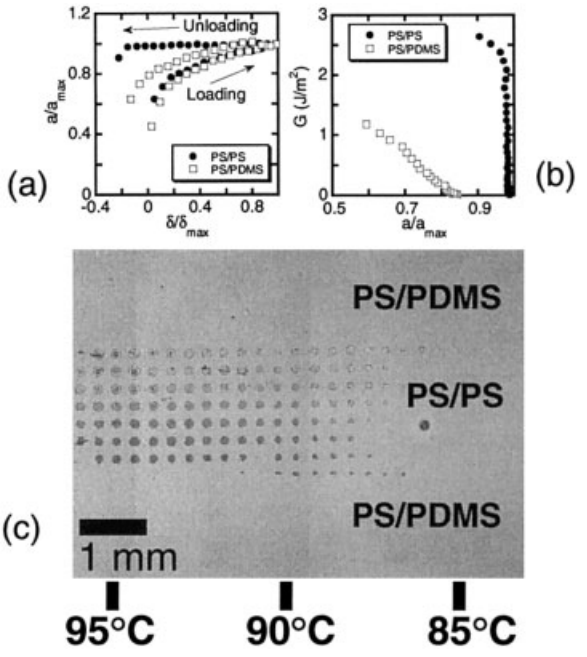

Figure 4. (a) Normalized contact history (δ/δ_{max} vs a/a_{max}) for PS/PS (●) and PS/PDMS (□) interfaces. Note the increase in hysteresis for the PS/PS interface. (b) Energy release rate ($\mathcal{G}$) versus normalized contact radius (a/a_{max}) for PS/PS (●) and PS/PDMS (□) interfaces during the unloading portion of the test. (c) Image of PS weld spots deposited on the PS-coated Si wafer after contact and separation of a PS-coated microlens array. The thickness of the PS coating on the Si wafer is 80 nm. The thickness of the PS coating on the PDMS microlens array is 216 nm. Temperature scale indicates the temperature of Si wafer substrate.

with shorter contacting times. This idea is demonstrated in Figure 2 where a sequence of images exhibits the hysteresis in contact history. In Figure 2(c) we used a simple simulation on the basis of the classical JKR theory to illustrate the qualitative mapping of surfaces with MCAT. For this simulation, we do not consider interlens coupling that occurs when the contact radius, a, becomes comparable to the interlens spacing. This interlens coupling has been investigated by Hui et al.[22] For our simulation, we controlled the displacement of a plane of soft, elastic, spherical caps contacting a flat, rigid plane. By defining the adhesion energy, $\mathcal{G}$, and the elastic modulus, E, of each lens, we iteratively calculate the contact radius and contact force for each lens. The resulting data for this simulation are presented as images of the contact areas for the contacting lens array as seen in Figure 2(c).

For these results, we defined a center region of the multilens array with a higher value of $\mathcal{G}$. The

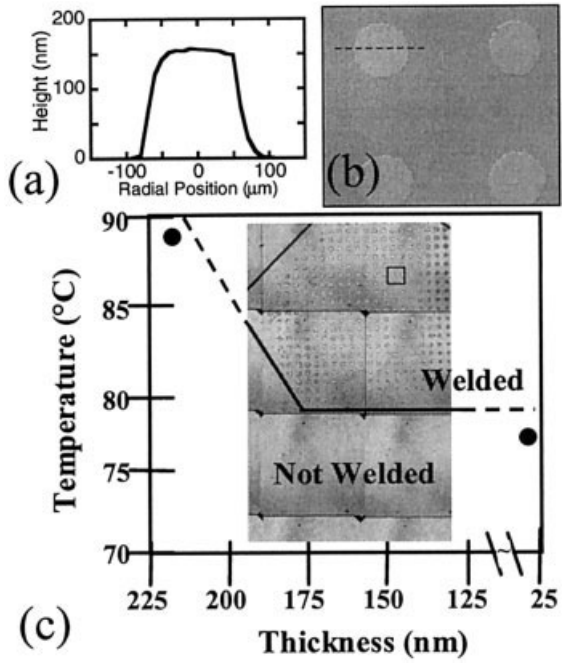

Figure 5. (a) Height profile of typical PS weld spot, (b) magnified image showing representative weld spots, and (c) image map of critical welding temperature dependence on thickness for the self-adhesion of PS thin films. Deposited weld spots indicate temperature and thickness regime where adhesive strength of PS/PS interface is greatest. PS-coated microlenses that contacted substrate below the solid line did not establish significant interfacial strength to sustain pull-off forces. Individual data points (●) collected by independent tests. Trendlines are not quantitative but are intended to guide the reader.

elastic modulus of all lenses was identical. We also defined the microlens array with a variance in lens height and a tilted alignment relative to the flat, "complementary" plane. These definitions simulate the conditions of our initial experiment where PS/PS interfaces have a higher adhesion at elevated temperatures and our planar alignment is nonideal. The time sequence in Figure 2(c) demonstrates the ability for MCAT to qualitatively distinguish regions of relatively higher adhesion across a surface of varying adhesive strength. In fact, the results of this simple simulation are nearly identical to the qualitative results of our PS/PS and PS/PDMS test depicted in Figure 2(b). Additionally, the simulation results indicate that ideal alignment between the two contacting surfaces is not required for qualitative measurements.

Likewise, a quantitative analysis can be used to determine the change in adhesion energy across our combinatorial library. With the measured quantities, contact radius (a) as a function of displacement (δ), and knowledge of bulk mechanical properties of the contact system, we have sufficient information to use eq 3 to determine the adhesion energy.

To demonstrate the analysis, we measure the contact history of the partially PS-coated PDMS microlens array with a PS-coated Si wafer fixed to a temperature-gradient stage (Fig. 4). Given the contact geometry for each individual microlens, we have a natural gradient in contact times within a contact area (Fig. 6). In other words, the outer regions of a contact area have the shortest contact times, whereas the maximum contact time is achieved in the center regions of each contact point. The gradient in contact time yields a gradient in interfacial strength within each contact area.

During the initial stages of unloading, $\mathcal{G}_o$ defines the applied energy-release rate at which interfacial fracture begins. For the PS/PS interfaces at 100 °C, we measure $\mathcal{G}_{o,PS/PS}$ to be 1.0

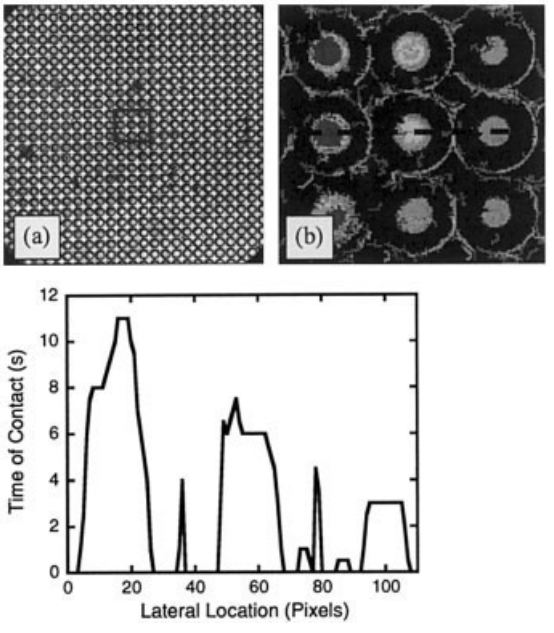

Figure 6. (a) Image of microlens array used in Figure 4 during contacting sequence. Highlighted box defines the region of analysis for parts (b) and (c). (b) Time-lapse image where color represents time of contact for a subarray of nine microlenses. A difference in time of contact exists across the array as well as within the contact history of a single microlens. (c) A line profile from the time-lapse image in part (b) defines the contact history of each microlens within the array.

$\pm$ 0.2 J/m^2 with a slight dependence on temperature. In contrast, we measure $\mathcal{G}_{o,PS/PDMS}$ as 0.02 $\pm$ 0.02 J/m^2 at 100 °C. For the setup used in these initial experiments, this measurement of $\mathcal{G}_{o,PS/PDMS}$ is below the lower limit of our resolution. Although our value for $\mathcal{G}_{o,PS/PDMS}$ is slightly less than the thermodynamic work of adhesion for this interface, the important point is that we measure a factor of 50 difference between the two interfaces. This factor of 50 indicates our ability to differentiate between the two interfaces on the same library, while also demonstrating the increased degree of entanglement at the symmetric polymer-melt interface relative to the melt/elastomer interface at short contact times.

For the PS/PS interfaces, the required driving force for interfacial failure increases as the center of the contact area is approached. Once the melt interface reaches a critical interfacial strength, fracture along the interface is energetically unfavorable. At this point, energy minimization is achieved by fracturing through the PS coating, thus causing a PS weld spot to be deposited onto the PS-coated Si wafer (Figs. 3 and 4). With the modified form of the JKR equation based on displacement, we calculated that the energy-release rate ($\mathcal{G}$) at which each weld spot was deposited is 3.8 $\pm$ 0.7 J/m^2, independent of weld-spot size (Fig. 5). As shown in Figure 4, the size of the weld spot decreases with decreasing temperature regardless of the fact that the maximum contact areas were uniform and independent of temperature. This temperature dependence on weld-spot size is related to either the critical time required to establish sufficient interfacial strength for coating failure or the temperature dependence of the PS coating strength.

The coating failure is essentially a tear mechanism (Fig. 7), and the tearing force through the coating will depend on coating thickness (analogous to tearing a single piece of article vs an entire pad of article). For a conventional tear test, the required tear force (F) varies linearly with the sheet thickness, h[23,24]

$$F = K_R h \tag{4}$$

The constant of proportionality, K_R, is referred to as the tear resistance, which is closely related to the material's fracture toughness. Previous research has demonstrated that the fracture toughness of a glassy polymer decreases with increasing temperature.[25,26] From our results for uniform thickness coatings (Fig. 4), we know that the critical interfacial strength, $\mathcal{G}$, for each weld spot does not change with the weld diameter. Accordingly, from eqs 2 and 3 we can determine the applied force (P) at weld deposition. This applied force at weld deposition is related to the tear force, F. From our results in Figure 4, an increasing tear force is required to deposit the weld spot for increasing temperature. Because this relationship contradicts the known temperature dependence for fracture toughness for PS, we can assume that the change in K_R with temperature is a minor effect relative to the time dependence of critical interfacial strength for determining the weld size.

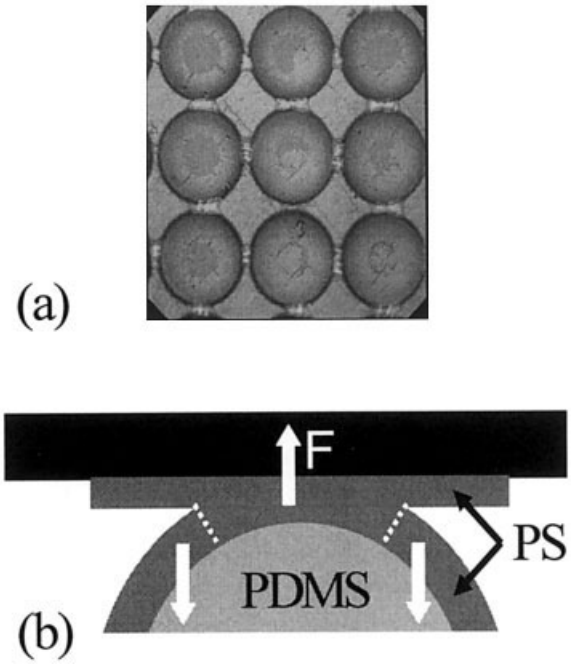

Figure 7. (a) Image of nine microlenses with PS coating completely or partially removed from deposition of weld spot. (b) Schematic demonstrating process of "tear" mechanism of PS coating during weld-spot deposition (not drawn to scale).

The fact that the area of the weld spots does not equal the maximum contact area indicates that the PS/PS interface near the edges of the maximum contact area (where contact time was the least) did not establish sufficient interfacial strength to fracture the PS coating. The interfacial strength of a symmetric polymer-melt interface is dictated by the density of molecules that cross, or "stitch," the interface and the extent of interpenetration. Previous theoretical and experimental results have suggested that this density

of interfacial links scales with $(t/\tau_{rep})^n$, where t is time of contact, τ_{rep} is the polymer molecule's reptation time, and n is 1/4 or 1/2 (depending on chain-end configuration at the precontact polymer surfaces).[27,28] If a critical entanglement density is achieved, then the coating will fail and a weld spot will be deposited. In accordance with previous results, the time to achieve this density will vary with temperature as indicated by the changing weld-spot size along the temperature-gradient axis.

This information is also important for understanding the results of our combinatorial experiment in Figure 5 that shows a T-h map where regions of greater film thickness ($h > 175$ nm) only weld at higher temperatures ($T > 78$ °C). This increase in welding temperature with thickness is related to either the increased tear force that is required to tear thicker regions of the PS coating or the thickness dependence of the T_g for thin polymer films. Although the short times for developing weld strength at temperatures below bulk T_g may be attributed to an increased near-surface molecular mobility,[29] the thickness dependence in Figure 5 is not dominated by molecular constraint. Previous research has demonstrated that molecular mobility of PS films is most significantly affected for a thickness less than 100 nm.[30] Our thickness dependence is introduced in films greater than 100 nm. Consequently, we believe the thickness dependence observed in Figure 5 is predominantly related to a thickness-dependent tear force.

According to eq 4, the increase in tear force is linearly proportional to the increase in coating thickness. If we consider K_R to be insignificantly dependent on temperature over our temperature range, then a 200-nm-thick coating will require a tear force 14% greater than the tear force for a coating of 175 nm (i.e., 200/175 = 1.14). To transmit this greater tear force, the PS/PS weld requires a greater interfacial strength because F–$P \sim \mathcal{G}^{0.5}$. Therefore, at higher temperatures and equivalent times of contact, our results indicate that a greater density of cross molecules is produced across the PS/PS weld to support the greater tear forces required for coating failure.

CONCLUSIONS

We have developed an adhesion-measurement technique to investigate the molecular origins of adhesion in a combinatorial manner. The technique that makes use of an array of microlenses and a modified form of the JKR theory allowed us to qualitatively and quantitatively map the interfacial adhesive strength across a surface. We have demonstrated this approach in the context of PS coatings and PDMS microlenses. Our test distinguished the relative differences in the adhesive strength of PS/PS and PS/PDMS interfaces at an elevated temperature, and mapped the trend of the critical PS/PS welding temperature as a function of PS-coating thickness. These results are potentially important for applications such as electronic packaging where thin films of glassy polymers are used to establish strong adhesive interfaces.

Temperature and coating thickness are only two examples of the variables that can be used in the combinatorial libraries. More generally, the methodology is useful for investigating the effect of multivariable environments (e.g., surface energy, crosslink density, surface roughness, and blend formulation) on polymer adhesion. A valuable benefit/advantage of the methodology is that all test points are exposed to the same test conditions, thus minimizing relative variations and allowing dominant controlling factors in adhesion to be rapidly isolated and determined. In addition to exploring parameter space, we can improve our library design by including internal standards and calibration points for quick assessment of relative properties. This high-throughput methodology is not only a powerful tool for industrial investigations where trends in adhesive behavior need to be quickly assessed, but the technique can also provide data under unique conditions for more fundamental investigations of molecular origins of polymer adhesion.

REFERENCES AND NOTES

1. Brocchini, S.; James, K.; Tangpauthadol, V.; Kohn, J. J Biomed Mater Res 1998, 42, 66.
2. Jandeleit, B.; Schaefer, D. J.; Powers, T. S.; Turner, H. W.; Weinberg, W. H. Angew Chem Int Ed Engl 1999, 38, 2494–2532.
3. Meredith, J. C.; Smith, A. P.; Karim, A.; Amis, E. J. Macromolecules 2000, 33, 9747–9756.
4. Meredith, J. C.; Karim, A.; Amis, E. J. Macromolecules 2000, 33, 5760–5762.
5. Johnson, K. L.; Kendall, K.; Roberts, A. D. Proc R Soc London A 1971, 324, 301–313.
6. Maugis, D.; Barquins, M. J Phys D: Appl Phys 1978, 11, 1989–2023.

7. Shull, K. R.; Ahn, D.; Chen, W.-L.; Flanigan, C. M.; Crosby, A. J Macromol Chem Phys 1998, 199, 489–511.
8. Tirrell, M. Langmuir 1996, 12, 4548–4551.
9. Ahn, D.; Shull, K. R. Langmuir 1998, 14, 3646–3654.
10. Ahn, D.; Shull, K. R. Langmuir 1998, 14, 3637–3645.
11. Barquins, M.; Maugis, D. J Adhes 1981, 13, 53–65.
12. Chuang, H. K.; Chiu, C.; Paniagua, R. Adhes Age 1997, 18–23.
13. Crosby, A. J.; Shull, K. R.; Lakrout, H.; Creton, C. J Appl Phys 2000, 88, 2956–2966.
14. Xia, Y.; Rogers, J. A.; Paul, K. E.; Whitesides, G. M. Chem Rev 1999, 99, 1823.
15. Xia, Y.; Whitesides, G. M. Angew Chem Int Ed Engl 1998, 37, 550.
16. Erdmann, L.; Efferenn, D. Opt Eng 1997, 36, 1094–1098.
17. Grunwald, R.; Mischke, H.; Rehak, W. Appl Opt 1999, 38, 4117–4124.
18. Haselbeck, S.; Schreiber, H.; Schwider, J.; Streibl, N. Opt Eng 1993, 32, 1322–1324.
19. Lu, Y.; Yin, Y.; Xia, Y. Adv Mater 2001, 13, 34–37.
20. Okamoto, T.; Mori, M.; Karasawa, T.; Hayakawa, S.; Seo, I.; Sato, H. Appl Opt 1999, 38, 2991–2996.
21. According to ISO 31–38, the term "molecular weight" has been replaced by "relative molecular mass," MR. The conventional notation, rather than the ISO notation, is used for this publication.
22. Hui, C. Y.; Lin, Y. Y.; Baney, J. M.; Kramer, E. J. J Polym Sci Part B: Polym Phys 2000, 39, 1195–1214.
23. Muscat-Fenech, C. M.; Atkins, A. G. Int J Fracture 1994, 67, 69–80.
24. Greensmith, H. W.; Thomas, A. G. J Polym Sci 1955, 18, 189–200.
25. Atkins, A. G.; Mai, Y. W. Elastic and Plastic Fracture, 1st ed.; Ellis Horwood, Ltd.: West Sussex, England, 1985, p 439.
26. Han, H. Z. Y.; McLeish, T. C. B.; Duckett, R. A.; Ward, N. J.; Johnson, A. F.; Donald, A. M.; Butler, M. Macromolecules 1998, 31, 1348–1357.
27. Gennes, P. G. d. Soft Interfaces, 1st ed.; Cambridge University Press: Cambridge, 1997, pp 79–95.
28. Bousmina, M.; Qiu, H.; Grmela, M.; Klemberg-Sapieha, J. E. Macromolecules 1998, 31, 8273–8280.
29. Koberstein, J. T. MRS Bull 1996, 21, 19–23.
30. Keddie, J. L.; Jones, R. A. L.; Cory, R. A. Europhys Lett 1994, 27, 59–64.